The Astrophysical Journal, 582:520–533, 2003 January 1

IDENTIFICATION OF SOLAR SOURCES OF MAJOR GEOMAGNETIC STORMS BETWEEN 1996 AND 2000

J. Zhang,[1] K. P. Dere,[2] R. A. Howard,[2] and V. Bothmer[3]

Received 2002 May 11; accepted 2002 September 6

ABSTRACT

This paper presents identification of solar coronal mass ejection (CME) sources for 27 major geomagnetic storms (defined by disturbance storm time index ≤ -100 nT) occurring between 1996 and 2000. Observations of CMEs and their solar surface origins are obtained from the Large Angle and Spectrometric Coronagraph (LASCO) and the EUV Imaging Telescope (EIT) instruments on the *SOHO* spacecraft. Our identification has two steps. The first step is to select candidate front-side halo (FSH) CMEs using a fixed 120 hr time window. The second step is to use solar wind data to provide further constraints, e.g., an adaptive time window defined based on the solar wind speed of the corresponding interplanetary CMEs. We finally find that 16 of the 27 (59%) major geomagnetic storms are identified with unique FSH CMEs. Six of the 27 events (22%) are associated with multiple FSH CMEs. These six events show complex solar wind flows and complex geomagnetic activity, which are probably the result of multiple halo CMEs interacting in interplanetary space. A complex event occurs when multiple FSH CMEs are produced within a short period. Four of the 27 (15%) events are associated with partial-halo gradual CMEs emerging from the east limb. The surface origin of these events is not known because of a lack of any EIT signature. We believe that they are longitudinally extended CMEs having a component moving along the Sun-Earth connection line. One of the 27 major geomagnetic storms is caused by a corotating interaction region. We find an asymmetry in the longitudinal distribution of solar source region for the CMEs responsible for major geomagnetic storms. They are more likely to originate from the western hemisphere than from the eastern hemisphere. In terms of latitude, most geoeffective CMEs originate within a latitude strip of $\pm 30^\circ$. The average transit time for a solar CME to arrive at the near-Earth space is found to be 64 hr, while it takes 78 hr on average to reach the peak of the geomagnetic storm. There is a correlation between CME transit time from the Sun to the near-Earth space (T, in hours) and the CME initial velocity (V, in unit of kilometers per second) at the Sun, which can be simply described as $T = 96 - (V/21)$. We also find that while these geoeffective CMEs are either full-halo CMEs (67%) or partial-halo CMEs (30%), there is no preference for them to be fast CMEs or to be associated with major flares and erupting filaments.

Subject headings: solar wind — Sun: corona — Sun: coronal mass ejections (CMEs) — Sun: flares

1. INTRODUCTION

This paper is intended to unambiguously identify solar sources of major geomagnetic storms based on a comprehensive set of solar, interplanetary, and geomagnetic observations. Coronal mass ejections (CMEs) from the Sun drive solar wind disturbances in terms of magnetic field, speed, and density, which in turn cause magnetic disturbances at the Earth. Geomagnetic storms have been found to be particularly sensitive to the presence of an intense southward interplanetary magnetic field that allows efficient energy transfer from the solar wind into the Earth's magnetosphere through magnetic reconnection (Dungey 1961; Fairfield & Cahill 1966; Gonzalez & Tsurutani 1987). Although this general idea of the solar cause of geomagnetic storms has been established for decades, the exact solar sources and their characteristics have not been well identified and studied until the advent of *Solar and Heliospheric Observatory* (*SOHO*) spacecraft observations in 1996.

In early studies, interplanetary solar wind data have been used to indirectly infer the nature of solar sources of geomagnetic storms. There are in general two kinds of solar sources, CMEs and corotating interaction regions (CIRs). The CME counterparts in interplanetary space, conventionally called interplanetary CMEs (ICMEs), can be verified by various solar wind signatures including magnetic clouds (Burlaga et al. 1981; Klein & Burlaga 1982) and bidirectional electron fluxes (Gosling et al. 1987). Other solar wind features can also be used as CME signatures (Richardson & Cane 1995). ICMEs are geoeffective because of either the enhancement of an interplanetary magnetic field compressed by CME-driven shocks or the presence of strong magnetic fields carried by CMEs themselves, or both (Bothmer & Schwenn 1998; Tsurutani 2001). CIRs are compressed solar wind structures that occur when a fast-speed stream originating in open magnetic field coronal holes catches up with a preceding slow-speed stream originating from a relatively closed magnetic structure (Smith & Wolfe 1976; Gosling & Pizzo 1999). Both CMEs and CIRs contribute to minor and moderate geomagnetic storms (Lindsay, Russell, & Luhmann 1995). Nevertheless, major geomagnetic storms are found to be mainly caused by CMEs (Gosling et al. 1990; Bothmer & Schwenn 1995; Tsurutani & Gonzalez 1998).

[1] Center for Earth Observing and Space Research, George Mason University, Fairfax, VA 22030.
[2] E. O. Hulburt Center for Space Research, Naval Research Laboratory, 4555 Overlook Avenue SW, Washington, DC 20375.
[3] Max-Planck-Institut für Aeronomie, Postfach 20, Katlenburg-Lindau D-37189, Germany.

A combination of remote sensing solar observations and in situ solar wind observations provides an integrated approach to the identification of the solar sources of geomagnetic storms. Earlier efforts to establish individual Sun-Earth connections have been based on presumed CME proxies, including disappearing solar filaments (Joselyn & McIntosh 1981; Rust 1994; Bothmer & Rust 1997), erupting features in X-ray coronal images (McAllister et al. 1996; Weiss et al. 1996), and long-duration soft X-ray flares (Sheeley et al. 1975; Landi et al. 1998). Since the advent of *SOHO*, a comprehensive approach has become possible due to the CME observations of the Large Angle and Spectrometric Coronagraph (LASCO; Brueckner et al. 1995) and coronal observations of the EUV Imaging Telescope (EIT; Delaboudinière et al. 1995). Recent studies (Brueckner et al. 1998; Webb et al. 2000) have established the geoeffectiveness of halo CMEs. Halo-type CMEs, first discovered by Howard et al. (1982), appear with a full or partial circular shape surrounding the Sun and presumably have a component moving along the Sun-Earth line. Statistical studies have found that the CME transit time from the Sun to the near-Earth space falls in between 1 and 5 days and coarsely depends on the CMEs' initial speed (Gopalswamy et al. 2000; Cane, Richardson, & Cyr 2000).

In this paper, we concentrate on identifying solar CME sources for major geomagnetic storms occurring between 1996 and 2000 inclusive. The identification process itself is not straightforward. Almost half of the major geomagnetic storms are not associated with a unique halo CME originating from front-side solar disk within a fixed time window. Some major geomagnetic storms may be associated with multiple CME sources. Complex solar wind flows (also called compound streams) have been reported before, and they are speculated to be caused by multiple CME interaction in interplanetary space (Burlaga, Behannon, & Klein 1987; Bothmer & Schwenn 1995). Direct CME interaction has been recently observed for limb CME events that show unusual radio signatures (Gopalswamy et al. 2001). On the other hand, some major geomagnetic storms are not associated with any front-side halo CME. They may be caused by puzzling "toroidal" halo CMEs (Brueckner et al. 1998; Webb et al. 2000). In order to find unambiguous solar sources of major geomagnetic storms, we make use of a two-step approach of identification. The first step is to find candidate halo CME sources within a fixed time window based on LASCO and EIT observations. The second step is to look into solar wind signatures to further constrain possible CME sources.

We also study the solar characteristics of the identified geoeffective CMEs in order to find out whether geoeffective CMEs bear special signatures among all CMEs. The study includes their velocity distribution, source region distribution on the Sun, and their association with other solar surface phenomena such as flares and filament eruptions. Transit times for solar CMEs to arrive at the near-Earth space and to the peak time of geomagnetic storms are also explored as well as their correlation with the CMEs' initial velocity. The paper is organized as follows: In § 2, we present the data and identification methods. In § 3, identification results and discussion about the results are presented. In § 4, we present and discuss solar characteristics of geoeffective CMEs. Conclusions are given in § 5.

2. DATA AND IDENTIFICATION METHODS

2.1. *Geomagnetic Storm, CME, and Fixed Time Window Method: First Step*

In the 5 yr period from 1996 January to 2000 December, 38 major geomagnetic storms have been observed based on the disturbance storm time (Dst nT) index. The Dst is derived from hourly horizontal magnetic variations recorded in a network of near-equatorial geomagnetic observatories. The variations of the horizontal-component field on the ground are believed to be caused by the changes in the global high-altitude equatorial ring current, which in turn depends on solar wind conditions. A geomagnetic storm is classified as a major storm if the index at the peak time is less than or equal to -100 nT. We note that the Kp index (3 hr 0–9 scale index measured by middle-latitude observatories, in contrast to the Dst by near-equatorial observatories) has also been used to measure the intensity of geomagnetic storms. There are a total of 28 major Kp events with $\mathrm{Kp} \geq 7$ in the 5 yr period investigated. Among the 38 Dst major events, 20 of them are also Kp major events. Clearly, there are significant differences between sets of major geomagnetic storms defined by the two indices. In this paper we use major geomagnetic storm events defined by the Dst index.

To identify the solar CME sources of these major geomagnetic storms, we make use of LASCO and EIT observations that started in 1996 January. LASCO consists of a set of three nested coronagraphs with overlapping, concentric fields of view: C1 (1.1–3 $R_\odot$), C2 (2–6 $R_\odot$), and C3 (4–30 $R_\odot$). The observations are primarily obtained with C2 and C3 with a combined field of view of 2–30 $R_\odot$; C1 ceased functioning after a 4 month long disruption of spacecraft operation in 1998. Compared with earlier space-based coronagraphs, LASCO has a larger field of view, better sensitivity, and high duty cycle, resulting in more frequent detection of halo CMEs. For the 5 yr period from 1996 January to 2000 December, about 3330 CMEs total were observed by LASCO. Among them, 309 CMEs (or 9.3%) are halo CMEs, which include 160 (or 4.8%) partial-halo CMEs (defined by angular width more than 140°) and 149 (or 4.5%) full-halo CMEs.

Because a halo CME can move either toward the Earth if initiated on the front side of solar disk or away if initiated on the back side, EIT observations play a necessary role in identifying the solar disk source region of a CME. The EIT instrument is a normal-incidence telescope with multilayer-coated mirrors making images of the Sun in four narrow EUV channels centered at 171, 195, 284, and 304 Å. EIT images cover the full solar disk and the corona up to 1.5 $R_\odot$ and complement LASCO's observations of the outer corona. EIT generally operates in a so-called CME watch mode that observes the corona in the 195 Å channel (sensitive to coronal plasma of 1.5 MK) with a cadence of 10–20 minutes, comparable with that of LASCO observations. A front-side halo CME is usually apparent in EIT images, as dimmings, waves, localized brightenings, or posteruption loop arcades. To associate a CME in C2 with coronal dimming in the EIT is often straightforward because the transit time for a CME from the EIT to the C2 is in the range of tens of minutes to a few hours depending on the speed. During such a period, usually only a single CME occurs, and a unique EIT dimming matches that CME. In addition, the heliocentric location of a dimming region seen in the EIT fits

well the position angle of the corresponding CME; e.g., a CME would have a position angle between 0° and 90° (angle measured counterclockwise from the northern pole) if the source region is on the northeast quadrant of the disk.

To associate a geomagnetic storm with a particular solar CME, we first choose a fixed 30–120 hr backward time window to look for candidate CMEs. In this first step, candidate CMEs are limited to front-side halo (FSH) CMEs, which are presumably the sources of major geomagnetic storms. The fixed time window method has been conveniently used by other workers to relate LASCO CMEs with geomagnetic storms (Brueckner et al. 1998; Webb et al. 2000) or CME counterparts in interplanetary space (Gopalswamy et al. 2000; Cane et al. 2000); the transit time has been found to be from 1 to 5 days. We note that there are two transit times available, one from the Sun to the spacecraft in the near-Earth space and the other from the Sun to the peak time of geomagnetic storms; the second transit time is hours later than the first one. The fixed 30–120 hr window here refers to the second transit time because we use the Dst peak time as the reference point. The chosen 120 hr upper bound window is large enough to include almost all CME candidates. It takes 119 hr for a solar CME to reach the near-Earth space if the CME moves at an average speed of 350 km s^{-1}, the lower end of observed solar wind speeds. Although rare, exceptional longer transitions can occur when a source CME is very slow close to the Sun and is gradually accelerated in the corona and maintains a low speed in the heliosphere; in this case, the upper window may be enlarged based on the subsequent consideration of solar wind and solar CME observations. We choose 30 hr as the lower bound of the time window. This requires an average transit speed of 1400 km s^{-1}, which is far larger than the upper end of observed solar wind speed. Based on events we have investigated so far, the shortest transit time turns out to be 34 hr, which is for the well-known 2000 July 14 CME event (see *Solar Physics Journal*, Volume 204, a special issue for this event).

We are able to identify the solar sources for all 27 events, which have complete and continuous observations in both LASCO and EIT. The other 11 events unfortunately occurred during either the *SOHO* operation disruption period (seven events; 1998 July to September, 1999 January) or the LASCO (three events) and EIT (one event) maintenance period. Within a 90 hr long window size, there are in general about four CMEs near solar minimum in 1997 and about 16 CMEs near solar maximum in 2000. Selection of only FSH CMEs results in a much smaller event list. We find that 15 (56%) of the 27 well-observed events have a unique FSH CME candidate. However, nine (33%) of the 27 events have multiple FSH CME candidates, and three (11%) of them have no FSH candidate. In the first row of Table 1, we list the number of storm events in each of the three categories, named as unique (*U*), multiple (*M*), and special (*S*; not attributed to an FSH CME).

TABLE 1
Number of Events in Three Identification Categories

Storm-CME Relationship	Unique (*U*)	Multiple (*M*)	Special (*S*)
Fixed time window.....	15 (56%)	9 (33%)	3 (11%)
Solar wind constraints.....	16 (59%)	6 (22%)	5 (19%)

2.2. *Solar Wind Data and Constraints: Second Step*

The nonunique association of almost half of the major geomagnetic storms with FSH CMEs raises the issue of ambiguity in the identification. Is there a single CME source for those storms associated with multiple CMEs? What is the solar source for those storms not associated with FSH CMEs? How confidently can a unique candidate CME be considered to be the true cause of a corresponding geomagnetic storm? To address these questions, a second step is introduced by exploiting the solar wind observations. In situ solar wind measurements reveal the characteristics of the CME counterpart in interplanetary space. The solar wind data we use in this paper are from plasma and magnetic field instruments on board *Wind* (Ogilvie et al. 1995; Lepping et al. 1995) and the *Advanced Composition Explorer* (*ACE*; McComas et al. 1998; Smith et al. 1998).

One obvious parameter from the solar wind data is the speed of the ICME, which can be used to calculate a maximum transit time from the Sun to the near-Earth space and adjust the upper bound of the time window. For instance, the upper bound of the time window would be reduced to as small as 69 hr when the speed of an ICME at near-Earth space is 600 km s^{-1}. In the presence of magnetic cloud in ICMEs, Bothmer & Schwenn (1994) used the minimum and maximum speed in the magnetic cloud to calculate the start and end of the time window. In this paper, we use the speed of the ICME front, which is often the well-defined shock front, to calculate the transit time. Thus, the calculated time is the maximum possible transit time for those CMEs that initially have a high speed at the Sun and maintain or decrease the speed in their course toward the Earth. This is based on the fact that the speed distribution of solar CMEs is much wider than that of ICMEs (Gopalswamy et al. 2000). Consequently a high-speed solar CME generally decelerates and a slow-speed solar CME accelerates during its course from the Sun to the Earth. Fast solar CMEs, which are also generally called impulsive CMEs, are found to be accelerated in the lower corona within tens of minutes in time and a few solar radii in distance but often maintain a constant speed or slightly decrease speed in the outer corona (Sheeley et al. 1999; Andrews & Howard 2001; Zhang et al. 2001). Therefore, an adaptive time window can be reasonably applied to candidate CMEs that are initially fast and associated with flares. However, we caution here that this method cannot be used for candidate CMEs that are initially slow and have gradual accelerating characteristics.

Besides the speed, other solar wind features are also important in constraining candidate CMEs. If the solar wind displays the presence of a simple ICME that is composed of a shock sheath and a magnetic cloud, the ICME would be considered to be the result of a single solar CME. On the other hand, if the solar wind shows complex flows such as multiple shocks and/or magnetic clouds, the ICME would be considered to be the result of multiple solar CMEs. The solar wind data are also used to identify CIRs as opposed to CMEs. By making use of both solar CME data and solar wind data, we reach the final identifications, which are believed to be unambiguous. We have made unique associations for two of the nine events that are originally associated with multiple CMEs in the fixed-window method. One event (on 2000 October 4), originally having three candidate CMEs, turns out to be not associated with any of them; this event is moved to the special category. For

those 15 events initially with unique CME candidates, we find that 14 of them fit solar wind constraints, and therefore the original candidate CMEs are very likely the true solar sources of geomagnetic storms; the other event (on 2000 August 11) is moved to the special category. After applying solar wind constraints, there are still three classes of events based on the number of FSH CMEs (unique, multiple, and none) associated with each geomagnetic storm. In the second row of Table 1, we list the total number of storm events for the three classes, which are now 16 (59%), six (22%), and five (19%), respectively. In the next section, we illustrate the detailed identification process using some events as examples.

3. IDENTIFICATION RESULTS AND DISCUSSIONS

3.1. *Major Geomagnetic Storms with Unique CME Source*

It is relatively straightforward to confirm the identification of the solar source CME for those 15 storm events originally associated with a unique candidate FSH CME within the 120 hr fixed time window. First, we look into solar wind data to check the existence of the corresponding single ICME. Second, we apply the adaptive time window method for those ICMEs with shock structure. We can confirm that, indeed, for 14 of the 15 events, the unique CME source in the 120 hr window is very likely the true source of corresponding geomagnetic storm. However, the storm event at 2000 August 11, 06:00 UT (Dst −103 nT) is an exception. It consists of two events with a second peak in Dst 27 hr later at August 12, 09:00 UT. The two storms share one candidate front-side halo CME (at August 9, 16:30 UT), which was ejected with a speed of 702 km s^{-1} from active region NOAA 9114 and associated with a *GOES* C2.3 flare at N11°W11°. The solar wind data show two distinct ICMEs, which arrive at the near-Earth space at August 10, 04:00 UT and August 11, 18:00 UT. We believe that the only candidate CME is the source of the second storm; it takes the CME 49 hr to arrive at the near-Earth space. This CME cannot be the source of the first storm because the transit time for the CME to the first ICME arrival would be only 11 hr, which is too short to be realistic. Therefore, the storm on 2000 August 11 must be caused by another CME that is not a front-side halo CME and will be investigated later.

We now explain how we make unique associations for two major geomagnetic storms that originally have multiple CME candidates in a fixed time window. The storm on 1997 November 7, 04 UT (Dst −110 nT) has two candidate front-side halo CMEs within the fixed 120 hr window: one occurred at 11:11 UT on November 3 and the other at 06:10 UT on November 4, with a temporal separation of 19 hr. The two CMEs are shown in the Figure 1 in the upper and lower panels. The EIT difference images (*left-hand panels*) show dimming/wave features indicating the CMEs' source location, and the C2 difference images (*right-hand panels*) show their morphology. The arrows in the C2 images point at CME leading edges in the southwestern portion. Both CMEs become full halo later in C3 images. They originate in the same active region (NOAA 8100). The first CME has an apparent speed of 369 km s^{-1} and is associated with a *GOES* M4.2 flare at S19°W12°, while the second CME has a speed of 830 km s^{-1} and is associated with a *GOES* X2.1 flare at S14°W33°. Based on solar CMEs only, we are not able to judge which of the two CMEs is the true source of the subsequent geomagnetic storm. We use the solar wind data to provide further constraints. In Figure 2, we plot the solar wind bulk velocity, density, ion temperature, magnetic field, and *X*-, *Y*-, and *Z*-components of magnetic field (all in geocentric solar ecliptic [GSE] coordinates) along with the DST index for a period of 4 days from November 6 to 10. The figure clearly shows the solar wind features of a single ICME, which is composed of a shock and a magnetic cloud. The shock front, indicated by the solid vertical line, arrived at 22:10 UT on November 6; at this moment, all major solar wind parameters including velocity, density, and magnetic field jump up. The magnetic cloud, whose 31 hr long period is indicated by the two dotted vertical lines following a 7 hr long shock sheath, starts at November 7, 05:00 UT and ends at November 8, 12:00 UT. The solar wind characteristics indicate a simple ICME, which should originate from a single CME. We then use the solar wind speed of the shock front (470 km s^{-1}) to calculate the maximum transit time from the Sun to the near-Earth space, which turns out to be 89 hr. The observed transit times of the two candidate CMEs from the Sun to the near-Earth space are 83 and 69 hr. The above numbers favor the second CME as the source because its transit time of 69 hr is well within the allowed maximum transit time of 89 hr. The first CME, although its transit time of 83 hr is also within the maximum time, may not be the source because the two times are very close; the maximum transit time calculated from the solar wind speed is believed to be a conservative one. Therefore, we conclude that the storm on 1997 November 7 is probably caused by the second CME on November 4, 06:10 UT.

Another case is the storm event on 1998 November 8. There are a pair of major geomagnetic storms consecutively occurring at November 8, 06:00 UT (Dst −149 nT) and November 9, 17:00 UT (Dst −142 nT) with a temporal separation of 35 hr. Within the 120 hr fixed window of the first storm, there are two front-side halo CME candidates, which occurred at November 4, 07:54 UT and November 5, 20:44 UT. The two CMEs, which originate in the same active region (NOAA 8375), are associated with *GOES* C1.6 (at N17°E01°) and M8.4 (at N22°W18°) flares and have apparent speeds of 527 and 1124 km s^{-1}, respectively. It is found that the second major geomagnetic storm is uniquely associated with the second CME within the 120 hr window. In the solar wind data, there appear two distinct ICMEs, each of which has shock and magnetic cloud structure. The two ICMEs arrived at November 7, 07:00 UT and November 8, 04:00 UT, with a separation of 21 hr; their solar wind velocities are 520 and 640 km s^{-1}, respectively. Because solar wind data show two distinct ICMEs and the second storm is uniquely associated with the second CME, we believe that the first CME is the cause of the first major storm. This a case in which two CMEs, which originate from the same active region, cause two consecutive but separate ICMEs in interplanetary space, which in turn cause two major geomagnetic storms.

Using these methods, we are able to make unique associations with front-side halo CMEs for 16 major geomagnetic storms among the 27 events investigated. In Table 2, we list the 16 unique events. From left to right, the columns represent the peak time of DST, the time of solar source CME, CME velocity, CME position angle, CME angular width (AW), CME source region type on the Sun's surface, heliocentric coordinates of solar surface source region, associated *GOES* soft X-ray flare, association with erupting

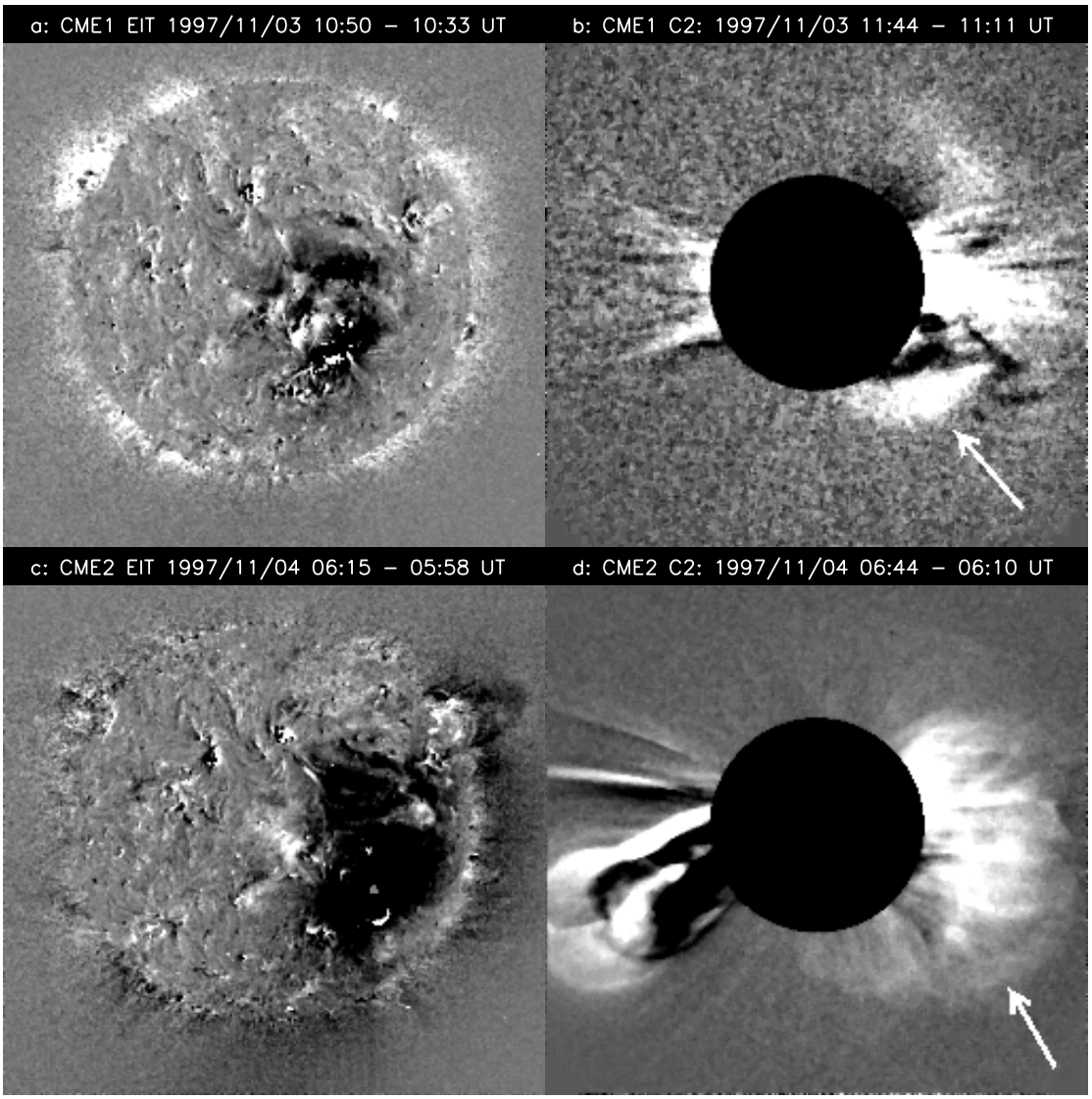

FIG. 1.—Display of two candidate solar CME sources for major geomagnetic storm on 1997 November 7. (*a*) and (*b*) EIT and C2 difference images for the CME at November 3, 11:11 UT. (*c*) and (*d*) EIT and C2 difference images for the CME at November 4, 06:10 UT. The arrows in the two C2 images point at CME leading fronts in the southeastern portion. The second CME is believed to be the source of the major geomagnetic storm.

filament, ICME arrival time at the spacecraft, ICME velocity, calculated maximum transit time (TTC) based on solar wind speed, transit time observed from solar CME to ICME arrival at the spacecraft (TTI), and transit time observed from solar CME to storm Dst peak time (TTS). Note that there is no valid solar wind data for the storm on 2000 July 15; the data from the in situ plasma and magnetic instruments were corrupted by the very intense particle flux immediately following the solar CME on 2000 July 14. The heliocentric coordinates of a solar surface source region of a CME are given by the position of the associated H_α flare. For those CMEs that are not associated with flares or whose H_α positions are not observed when they occur close to the limb, we use the EIT dimming location to denote the CME source region position. Because CMEs are a large-scale phenomena, the designated heliocentric coordinates are good enough to serve the purpose of locating a CME origin on the solar disk. Whether a CME is associated with a filament/prominence or not is largely based on EIT observations, in which an erupting filament can be found as a moving dark feature against the background bright disk. We also check the synoptic H_α observations that report filament disappearance.

3.2. *Geomagnetic Storms with Multiple CMEs and Complex Solar Wind Flow*

In Table 3, we list the six major geomagnetic storms that we associate with multiple front-side halo CMEs. The storm line in the table designates the Dst peak time, ICME velocity, calculated maximum transit time, and ICME arrival time at the near-Earth space; each CME line designates the solar CME time, solar CME velocity, observed transit time from the Sun to the near-Earth space, CME position angle, CME angular size, CME source region type, CME source region location, associated *GOES* X-ray flare magnitude, and association with erupting filaments. We are not able to make a unique association for these events even after exploiting solar wind data to impose additional constraints. Nevertheless, the numbers of candidate CMEs are smaller

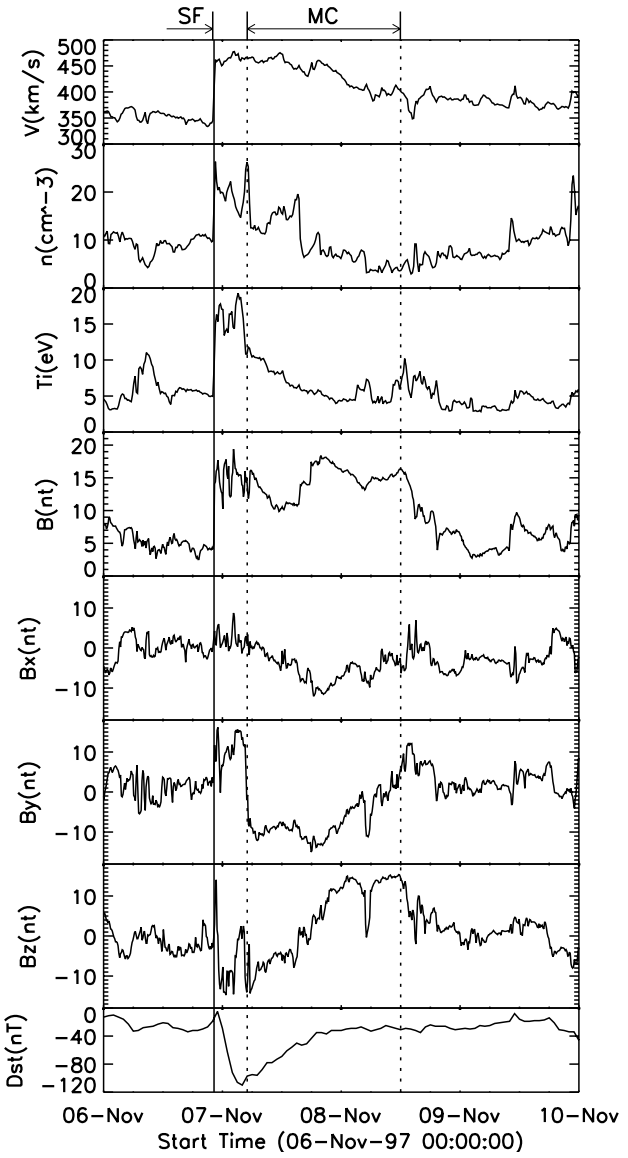

FIG. 2.—Solar wind plot for the major geomagnetic storm on 1997 November 7. From top to bottom the panels plotted are the plasma velocity, density, ion temperature, magnetic field strength, magnetic field strength in the *X*-, *Y*-, and*Z*-components (above parameters are all in GSE coordinate), and Dst index, respectively. The vertical solid line indicates the time of the ICME arrival (the shock front) at the *Wind* spacecraft situated in the near-Earth space. The two vertical dotted lines indicate the starting and ending time of the magnetic cloud component of the ICME.

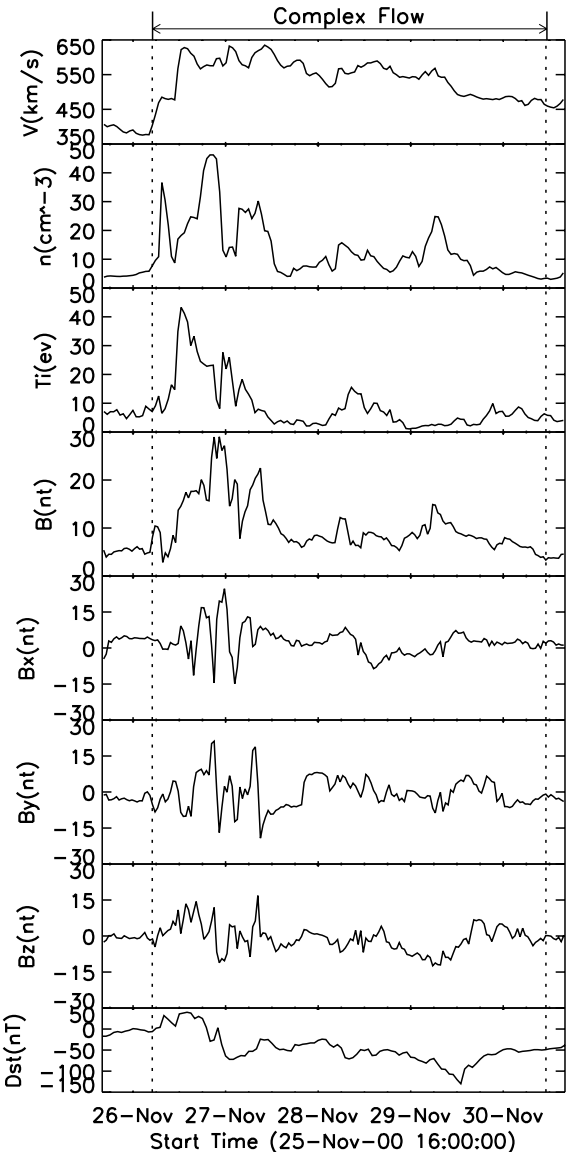

FIG. 3.—Solar wind plot for the major geomagnetic storm on 2000 November 29. Note that the solar wind flow is a complex one, very likely caused by multiple solar CMEs interacting in interplanetary space. The two vertical dotted lines indicate the starting and ending time of the complex flow. The data are from the *ACE* experiment.

than those obtained with the fixed time window method. The solar wind structure of these geomagnetic storms often shows a complex flow that cannot be simply decomposed into individual ICMEs or transient flows.

We use the major geomagnetic storm on 2000 November 29 (Dst −130 nT) as an example to illustrate characteristics of this kind of complex event. Within a fixed 120 hr time window, the 2000 November 29 storm originally has seven candidate front-side halo CMEs. For a solar wind speed of 570 km s^{-1}, the calculated maximum transit time is reduced to 73 hr, which however, still includes four candidate CMEs (see Table 3). Three of the four CMEs are from the same active region NOAA 9236, which is very CME productive as it traverses across the visible solar hemisphere. The solar wind flow following this series of halo CMEs is very complex (Fig. 3). The complex flow lasts almost 100 hr (the interval between the two dotted lines in the figure, from November 26, 05:00 UT to November 30, 11:00 UT), which is much longer than a typical ICME flow. The Dst index maintains a moderate storm level for almost 2 days without recovery and plunges into major geomagnetic storm level on the third day. The complex flow is likely to be a composite result of multiple CMEs interacting and merging in interplanetary space.

The other five events in this multiple CME category show similar characteristics: complex geomagnetic activity and complex solar wind flow. About 22% of all major geomagnetic storms (six of 27) fall into this category, indicating that it is fairly important component. The typical solar source of this kind of event is highly CME-productive solar active regions that produce multiple Earth-directed halo CMEs within a relatively short period. These active regions are

TABLE 2

MAJOR GEOMAGNETIC STORMS ASSOCIATED WITH UNIQUE FRONT-SIDE HALO CMES

Dst (UT)	CME (UT)	Velocity ($km\ s^{-1}$)	P.A. (deg)	AW (deg)	Source	Coordinates (deg)	Flare	Filament	ICME (UT)	Velocity ($km\ s^{-1}$)	TTC[a] (hr)	TTI[b] (hr)	TTS[c] (hr)
1997 May 15 12:00	1997 May 12 06:30	306	Halo	360	AR 8038	N21W06	C1.3	No	1997 May 15 00:00	500	83	66	78
1997 Oct 11 03:00	1997 Oct 6 15:28	352	141	150	Quiet	S54E46	No	Yes	1997 Oct 10 15:00	480	87	96	108
1997 Nov 7 04:00.....	1997 Nov 4 06:10	830	Halo	360	AR 8100	S14W33	X2.1	No	1997 Nov 6 22:00	600	69	64	70
1998 Nov 8 06:00.....	1998 Nov 4 07:54	527	Halo	360	AR 8375	N17E01	C1.6	No	1998 Nov 7 07:00	520	80	71	94
1998 Nov 9 17:00.....	1998 Nov 5 20:44	1124	Halo	360	AR 8375	N22W18	M8.4	No	1998 Nov 8 04:00	640	65	55	92
1998 Nov 13 21:00.....	1998 Nov 9 17:54	353	324	192	Quiet	N10E20	No	No	1998 Nov 12 23:00	410	102	77	99
1999 Sep 22 23:00	1999 Sep 20 06:06	604	Halo	360	Quiet	S24E13	C2.2	Yes	1999 Sep 22 12:00	610	68	54	65
1999 Oct 22 06:00	1999 Oct 18 00:06	371	177	169	Quiet	S40E05	C1.2	Yes	1999 Oct 21 15:00	500	83	87	102
2000 Apr 7 00:00	2000 Apr 4 16:32	1188	Halo	360	AR 8933	N16W66	C9.7	Yes	2000 Apr 6 15:00	600	69	46	55
2000 May 24 08:00	2000 May 21 12:06	671	244	140	Quiet	S10W80	No	Yes	2000 May 23 16:00	600	69	52	68
2000 Jul 15 21:00	2000 Jul 14 10:54	1674	Halo	360	AR 9077	N22W07	X5.7	Yes	...	...	...	...	34
2000 Aug 12 09:00	2000 Aug 9 16:30	702	Halo	360	AR 9114	N11W11	C2.3	Yes	2000 Aug 11 18:00	680	61	50	65
2000 Oct 14 14:00	2000 Oct 9 23:50	798	Halo	360	AR 9182	N01W14	C6.9	No	2000 Oct 12 21:00	460	91	69	111
2000 Oct 29 02:00	2000 Oct 25 08:26	770	Halo	360	AR 9201	N18W23	C4.0	No	2000 Oct 28 05:00	440	95	69	90
2000 Nov 6 21:00.....	2000 Nov 3 18:26	291	Halo	360	AR 9213	N02W02	C3.2	No	2000 Nov 6 09:00	600	69	63	75
2000 Nov 10 12:00.....	2000 Nov 8 23:06	1345	Halo	360	AR 9217	N10W77	M7.4	No	2000 Nov 10 06:00	600	69	31	37

[a] TTC: maximum transit time calculated based on observed ICME speed.

[b] TTI: transit time observed from solar CME to ICME arrival at the near-Earth space.

[c] TTS: transit time observed from solar CME to the storm peak time.

TABLE 3
MAJOR GEOMAGNETIC STORMS ASSOCIATED WITH MULTIPLE CMEs

Storm/ CMEs	Date	Velocity (km s^{-1})	Transit Time[a] (hr)	ICME (UT)	P.A. (deg)	AW (deg)	Source	Coordinates (deg)	Flare	Filament
Storm.....	1998 May 4 05:00	800	52	1998 May 4 02						
CME1	1998 May 1 23:40	632	50		Halo	360	AR 8210	S18W05	M1.1	No
CME2	1998 May 2 05:31	452	44		Halo	360	AR 8210	S20W07	C5.4	No
CME3	1998 May 2 14:06	1044	36		Halo	360	AR 8210	S15W15	X1.1	No
Storm.....	1998 May 5 04:00	640	65	1998 May 6 00						
CME1	1998 May 2 05:31	452	66		Halo	360	AR 8210	S20W07	C5.4	No
CME2	1998 May 2 14:06	1044	58		Halo	360	AR 8210	S15W15	X1.1	No
Storm.....	2000 Feb 12 11:00	600	69	2000 Feb 11 23						
CME1	2000 Feb 9 19:54	910	51		Halo	360	AR 8853	S17W40	C7.4	Yes
CME2	2000 Feb 10 02:30	944	44		352	250	AR 8858	N17E01	C7.3	No
Storm.....	2000 Sep 17 23:00	860	48	2000 Sep 17 15						
CME1	2000 Sep 15 15:26	481	48		Halo	360	AR 9165	N12E07	M2.0	No
CME2	2000 Sep 15 21:50	257	41		Halo	360	AR 9165	N12E04	C7.0	No
CME3	2000 Sep 16 05:26	1232	34		Halo	360	AR 9165	N12W07	M5.9	No
Storm.....	2000 Oct 5 13:00	540	77	2000 Oct 5 09						
CME1	2000 Oct 2 03:50	465	77		171	360	AR 9176	S09E07	C4.1	No
CME2	2000 Oct 2 20:26	525	61		185	360	AR 9176	S09E00	C8.1	No
Storm.....	2000 Nov 29 13:00	570	73	2000 Nov 28 05						
CME1	2000 Nov 25 09:30	675	67		Halo	360	AR 9236	N18W24	M3.5	No
CME2	2000 Nov 25 19:31	671	57		Halo	360	AR 9236	N20W23	X1.9	No
CME3	2000 Nov 26 03:30	495	49		259	188	Quiet	S30W40	No	No
CME4	2000 Nov 26 17:06	980	36		Halo	360	AR 9236	N18W38	X4.0	No

[a] The transit time for the storm is TTC. The transit time for the CME is TTI.

more likely to occur during solar maximum than solar minimum. Complex solar wind flows (also called compound streams) have been reported and analyzed before (Burlaga et al. 1987; Bothmer & Schwenn 1995). These authors have suggested that complex flows are caused by multiple CMEs interacting in the interplanetary space, which is consistent with our findings. Although we are not able to directly observe the interaction between halo CMEs, CME interaction has been observed for limb CMEs and shows unusual radio signatures (Gopalswamy et al. 2001). We can infer from solar CME observations that the interaction in interplanetary space is inevitable due to fast-halo CMEs overtaking slower ones. Another complexity is the occurrence of twin major geomagnetic storms that appear consecutively within a short period (e.g., 24 hr). We refer to those as a storm pair. There are four such pairs among the 27 events investigated.

3.3. *Major Storms with CMEs of Unknown Source Region*

The major geomagnetic storms discussed so far are all associated with front-side halo CMEs. Such a connection is expected. However, there are five events that do not have any front-side halo CME candidate in the expected time window. These events are intriguing when one considers the implication for predicting major geomagnetic storms. We carefully investigate all available observations of solar surface, corona, and solar wind for these events in order to determine their solar sources. We conclude that four of them are caused by partial-halo gradual CMEs visible at the east limb. However, none of these CMEs have any surface signature in the EIT observations. These four events are listed in Table 4. For each event, the first line designates the Dst peak time, ICME velocity, calculated maximum transit time, and ICME arrival time at the spacecraft; the second

TABLE 4
MAJOR GEOMAGNETIC STORMS WITH EAST LIMB GRADUAL CMEs

Storm/ CME	Date (UT)	Velocity (km s^{-1})	Transit Time[a] (hr)	ICME (UT)	P.A. (deg)	AW (deg)	Source
Storm.....	1997 Apr 21 23:00	430	97	1997 Apr 21 06			
CME	1997 Apr 07:35	247	118		118	145	Unknown
Storm.....	1998 Feb 18 00:00	420	99	1998 Feb 17 04			
CME	1998 Feb 14 06:55	138	69		137	206	Unknown
Storm.....	2000 Aug 11 06:00	480	87	2000 Aug 10 04			
CME	2000 Aug 6 18:30	233	81		105	122	Unknown
Storm.....	2000 Oct 4 19:00	450	93	2000 Oct 4 00			
CME	2000 Sep 29 21:50	173	98		114	274	Unknown

[a] The transit time for the storm is TTC. The transit time for the CME is TTI.

line designates the solar CME time, solar CME speed, observed transit time from the Sun to the near-Earth space, solar CME position angle and width, and the surface source indicated as "unknown."

The first such event is the major geomagnetic storm on 1997 April 21, 23 UT (Dst −107 nT). The solar wind data show the presence of a magnetic cloud (Fig. 4, between two dotted lines), which unambiguously indicates that the cause will be a solar CME. The magnetic cloud is slow and long but not accompanied by a shock. There is no front-side halo CME occurring in a 5 day time window based on continuous LASCO/EIT observations. Indeed, the Sun is very quiet during the window. From April 17 to 19, no single CME has occurred. On April 20, there is one slow and very narrow CME (angular width 48°), which is unlikely to be the source. On April 16, two CMEs occurred, one at 07:35 UT, a partial-halo CME with an angular size of 145°, and the other at 01:34 UT with an angular size of only 41°. The most plausible solar source of this storm would be the CME at April 16, 07:35 UT (shown in Fig. 5). It is a very slow and gradual CME emerging from the east limb at a position angle of 118°. Its angular size slowly increases from an initial 90° to more than 140°, and its southern leading edge eventually sweeps through the southern pole. Its projected velocity gradually increases from tens of kilometers per second to about 250 km s^{-1} within a period of about 16 hr (at the final discernible height of 12 $R_{\odot}$). There is nothing in the EIT data to indicate where this gradual CME originated. The lack of an EIT signature of the CME would have been interpreted as the source being the CME is behind the limb and thus not considered a likely candidate for producing geomagnetic storms. However, now the presence of the magnetic cloud in the solar wind strongly suggests that the CME may be the source of the major geomagnetic storm; there is no other alternative source in the appropriate window.

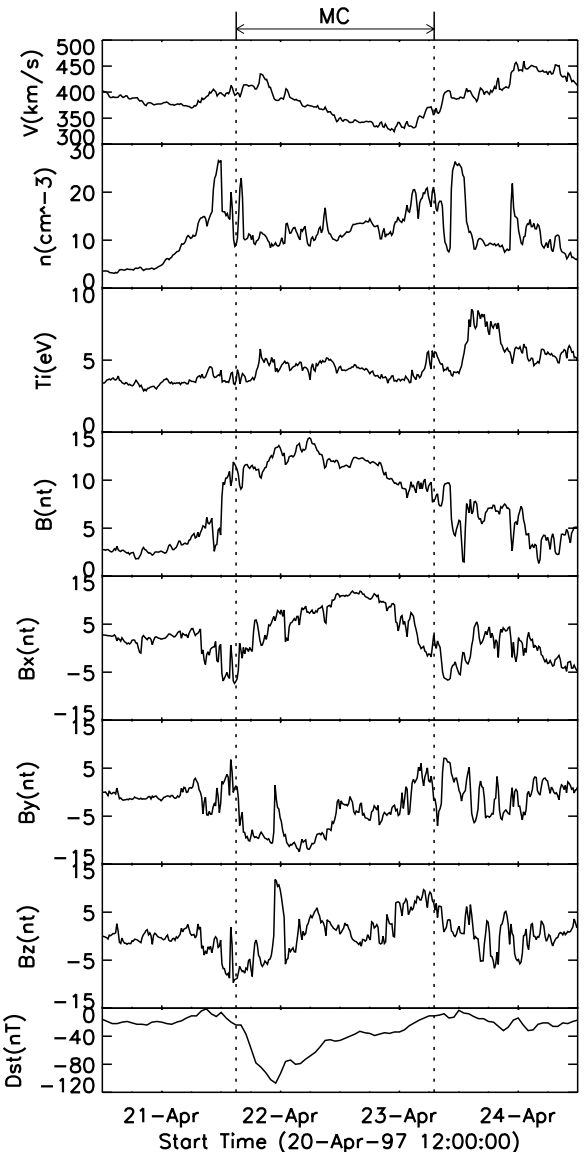

FIG. 4.—Solar wind plot for the major geomagnetic storm on 1997 April 21. The two vertical dotted lines indicate the duration of the associated magnetic cloud. Note that this ICME, which has a slow and long-period magnetic cloud but no shock, is probably caused by a longitudinal extended gradual CME emerging from the east limb. The solar wind data are from the *Wind* experiment.

The major geomagnetic storm on 1998 February 18 (Dst −100 nT) is very similar to the previous example in terms of both solar wind ICME and solar CME characteristics. The solar wind data show an unusually slow and long-duration magnetic cloud and the absence of a shock. There is no front-side halo CME in the time window. Nevertheless, we do find a partial-halo gradual CME emerging from the east limb starting at February 14, 07:00 UT. The CME slowly increases its speed to 160 km s^{-1} within a period of 10 hr. In the meantime, it slowly increases its angular width to about 200° and eventually sweeps across the southern pole. The similarity between this event and the previous one strengthens our view that the partial-halo gradual CMEs from the east limb are the solar sources of major geomagnetic storms.

The solar sources of the major geomagnetic storms on 2000 August 11 (Dst −103 nT) and October 4 (Dst −146 nT) also appear to be partial-halo gradual CMEs from the east limb. The identified CME sources are at 2000 August 6, 18:30 UT (position angle 105°, angular width 122°, speed 233 km s^{-1}) and 2000 September 29, 21:50 UT (position angle 114°, angular width 274°) surrounding the solar equator. Webb et al. (2000) further suggested that a "toroidal CME" can be geoeffective. Our observations support their concept. Nevertheless, we think the term "toroidal CMEs" is not accurate because we have not observed simultaneous activity on the other limb for the four events we investigated. We refer to them as longitudinal extended CMEs.

3.4. *A Major Geomagnetic Storm Caused by a CIR*

One major geomagnetic storm, the event on 1996 October 23, 04 UT (Dst −105 nT), does not seem to be caused by a CME. The solar wind data show no signature of an ICME (Fig. 6). Instead, they show a typical CIR feature. The CIR's stream interface, which separates the slow and dense plasma from the following fast and tenuous plasma, is identified in the solar wind data (see the vertical solid line in Fig. 6). The abrupt rise of ion temperature at the interface is another feature of a CIR. It is believed that the CIR is caused by a fast stream from a low-latitude coronal hole seen in the EIT images. Otherwise, the Sun is very quiet without an active region on the disk. There are no front-side halo CMEs in the time window. We conclude that the storm on 1996 October 23 is caused by a CIR instead of a CME.

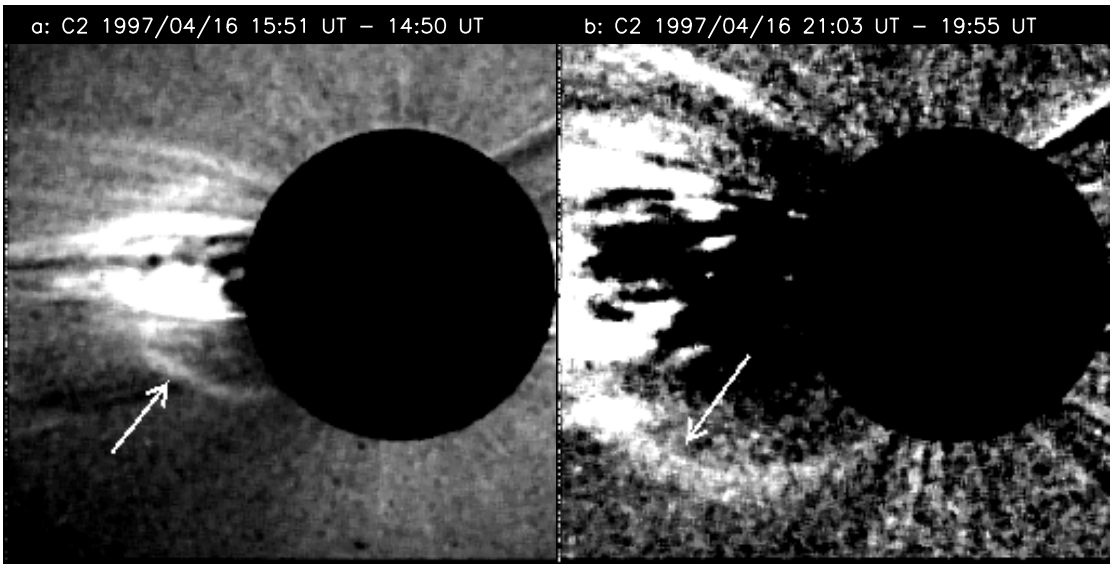

FIG. 5.—Partial-halo gradual CME at 1997 April 16, 07:35 UT. The two panels show C2 difference images. The arrows point at the southeastern portion of the CME leading edge. Note that the two images are taken 5 hr apart, which indicates the very slow motion of the CME leading edge. This CME is probably the source of the major geomagnetic storm on 1997 April 21.

The event of 1996 October 23 is the only event having a CIR source among the 27 events investigated. Bothmer & Schwenn (1995) also reported that one of 43 major geomagnetic storms occurring from 1966 to 1990 was caused by a CIR, but the other 42 events were caused by ICMEs. Therefore, a CIR is only occasionally the source of a major geomagnetic storm. Nevertheless, through their highly fluctuating magnetic field, CIRs can contribute to the cause of minor and moderate geomagnetic storms (Lindsay et al. 1995; Tsurutani 2001).

3.5. *CME Transit Time and Correlation with Solar CME Speed*

In Figure 7, we plot histograms of the transit time from solar CME to ICME arrival at the near-Earth space (Fig. 7*a*), the transit time from solar CME to Dst peak time (Fig. 7*b*), and the delay time between ICME arrival at the near-Earth space and Dst peak time (Fig. 7*c*) for the 26 events associated with CMEs. The average transit time from solar CME to ICME arrival at the near-Earth space is found to be 64 hr, with a maximum of 118 hr and minimum of 34 hr; the most probable transit time as seen in the peak of the histogram is 50–70 hr. The time from solar CME to Dst peak time is found to be 78 hr on average with a maximum of 135 hr and minimum of 34 hr. Note that the exceptional long 135 hr transit time from the Sun to the storm peak time is for an east-limb gradual CME. The other 25 events all have a transit time less than 120 hr. This confirms the usage of the 120 hr window rule to select candidate FSH CMEs in the first step.

There is a dear delay between ICME arrival time at the near-Earth space and the Dst peak time. The delay is understandable because the occurrence of a geomagnetic storm depends on the presence of a southern magnetic field, while the southern magnetic field can appear later in the ICME. The delay is 18 hr on average with a maximum of 40 hr and a minimum of 3 hr; the most probable delay time is 10–20 hr. When the southern magnetic field immediately follows the shock front, a short delay would occur. When the southern field appears in the rear of the magnetic cloud, a long delay would occur. In most cases of our study, the southern field appears at the end of the shock sheath and the front of the magnetic cloud.

In Figure 8, we plot the correlation between the CME transit time (from the Sun to near-Earth space) and the velocity of CMEs measured at the Sun. Note that the velocity is determined by linearly fitting the height-time measurement of CME leading edges in the C2/C3 images. Also note that such measured CME velocity is the projected velocity on the plane of the sky, which may be different from the true radial speed. Our correlation, which is for geoeffective CMEs, seems higher than the correlations obtained for general front-side halo CMEs (Cane et al. 2000; Gopalswamy et al. 2000). The linear fit (solid line in Fig. 8) gives a relation between transit time T (in hours) and CME velocity V (in units of kilometers per second) of

$$T = 96 - \frac{V}{21}\,. \tag{1}$$

The standard deviation of the fit is ± 13 hr. A linear fit to the relation with a negative coefficient implies that, on average, a CME decelerates in the interplanetary space. One may use this simple formula to calculate, with a first-order approximation, the arrival time of a CME at the near-Earth space. This formula is most accurate for fast events (e.g., >500 km s^{-1}).

4. SOLAR CHARACTERISTICS OF GEOEFFECTIVE CMEs

Having identified the solar CMEs and a single CIR responsible for 27 major geomagnetic storms occurring in a 5 yr period, we now present certain characteristics of these geoeffective CMEs and the implications for predicting major geomagnetic storms.

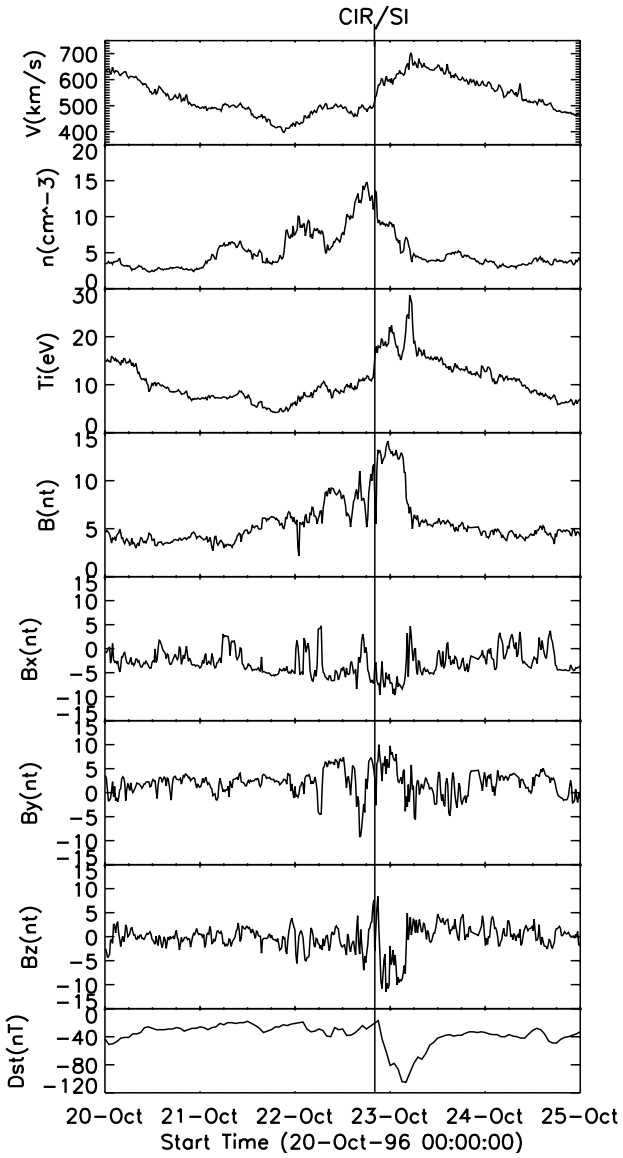

FIG. 6.—Solar wind plot for the major geomagnetic storm on 1996 October 23. The storm is caused by a CIR, whose stream interface is indicated by the solid line. The solar wind data are from the *Wind* experiment.

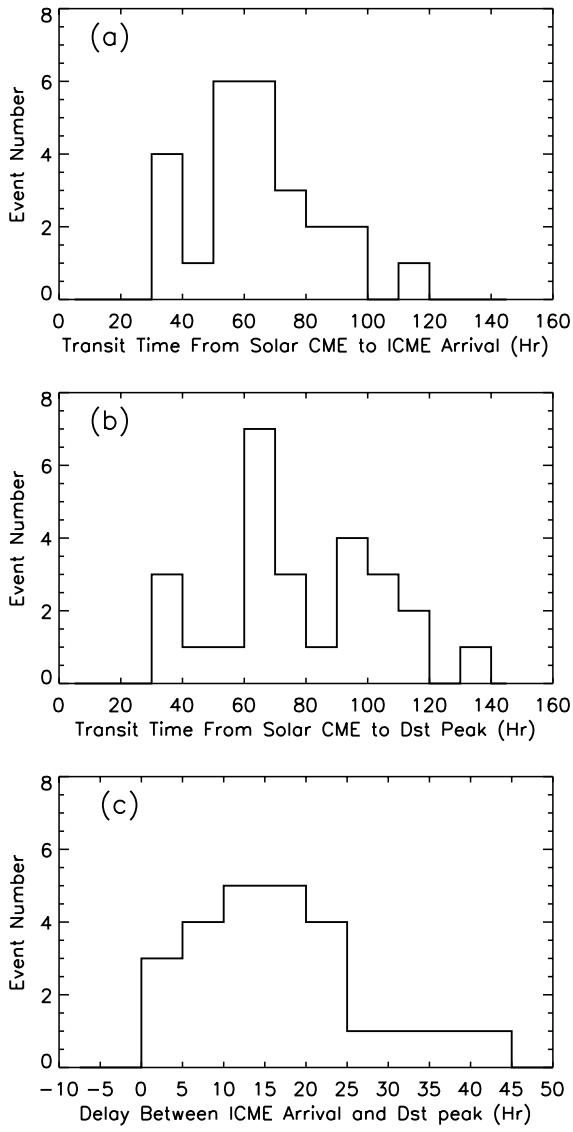

FIG. 7.—Histogram distribution of the CME transit times. (*a*) From solar CME to ICME arrival at the near-Earth *Wind* or *ACE* spacecraft. (*b*) From solar CME to the Dst peak time. (*c*) From ICME arrival at the spacecraft to the Dst peak time.

4.1. *Solar Surface Source Region Distribution of Geoeffective CMEs*

In Figure 9, we plot the heliocentric coordinates of the solar surface source region of the geoeffective CMEs. The events associated with unique front-side halo CMEs (16 events), multiple front-side halo CMEs (six events), and east-limb gradual CMEs (four events) are indicated in the figure. The source region location of a solar CME is based on the reported position of the H_α flare associated with the corresponding CME or the position of the associated EIT dimming region if no flare is reported. For multiple events, we choose the source region location of the last CME; the source region location of all candidate CMEs are usually close because they often come from the same active region (see Table 3). For the east-limb events, we use the CME position angle as the source region latitude and -90° as the longitude.

In terms of latitude, geoeffective CMEs originate within a latitude strip between S50° and N30°. In particular, a majority of events, 20 of 22 FSH CMEs, are from a latitude strip of $\pm 30^\circ$; 17 of the 20 events originated from active regions. The other two events, which are below S30°, are from the southeast disk quadrant and are not associated with active regions. This latitude distribution may simply follow the distribution range of active regions. It has been found that most CMEs (about 85%) are associated with active regions, while a small percentage (about 15%) are from quiet-Sun regions (Subramanian & Dere 2001).

In terms of longitude, we observe a longitudinal asymmetry in the distribution of the source region: geoeffective CMEs are more likely to originate from the western hemisphere than from the eastern hemisphere. Excluding the four limb events of unknown surface source, geoeffective CMEs cover a longitudinal range from E50° to W80°; most of them (17 of 22, or 77%) are within a narrower longitudinal range from E20° to W50°. Fifteen of the 22 events (68%) are from the western hemisphere, only four of the 22 events (18%) are from the eastern hemisphere, and the other three

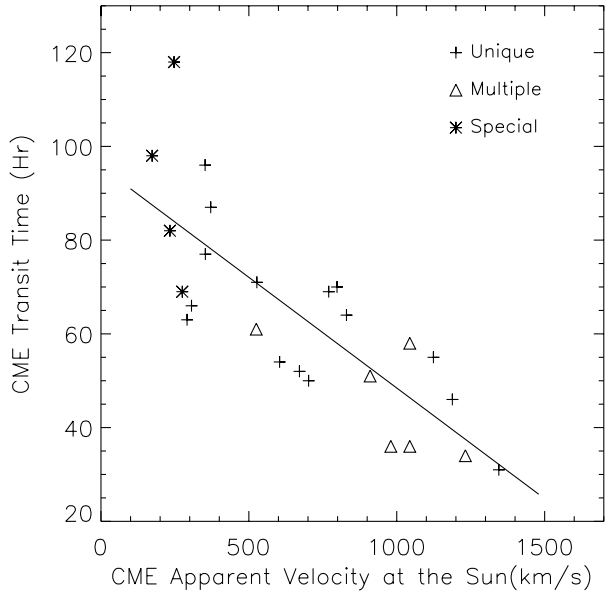

FIG. 8.—Correlation between the CME transit time (from the Sun to the ICME arrival at the near-Earth space) and the CME initial velocity at the Sun. The solid line shows a linear correlation fit.

events (14%) are close to the central meridian (within ±5°). Another way to describe the asymmetry is that the center of the source region distribution seems to be offset about 15° to the west. This longitudinal asymmetry is a new finding. It is in contrast with the survey of Cane et al. (2000), who found that Earth-impacting halo CMEs seem evenly distributed in longitude. Because geoeffective CMEs, which require the presence of prolonged southern magnetic field, are a subset of all Earth-impacting CMEs, the longitudinal asymmetry may be related with the well-known magnetic connection between the western solar hemisphere and the Earth orbit due to the background spiral magnetic field in the interplanetary space. The shock accompanying an ICME originating from the western hemisphere may have a better chance to reach the Earth following the spiral field than that originating from the eastern hemisphere.

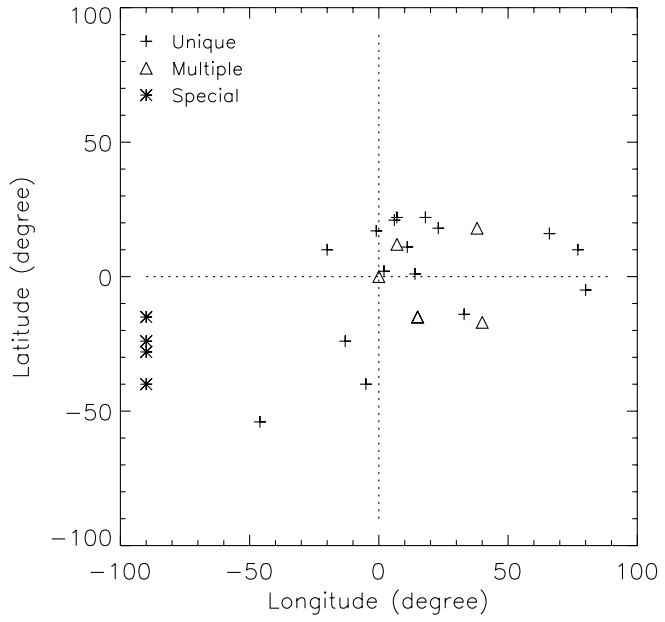

FIG. 9.—Distribution of heliocentric coordinates of the solar surface source region of the geoeffective CMEs that cause major geomagnetic storms. The signs indicate storm events identified to be caused by a unique front-side halo CME (*plus sign*), multiple front-side halo CMEs (*triangle*), and east-limb gradual CMEs with an unknown surface source (*asterisk*; special).

4.2. *Lack of Distinguished Solar Manifestation for Geoeffective CMEs*

In this section, we discuss practical issues regarding the prediction of major geomagnetic storms based on CMEs' solar manifestation. First, we point out that only a very small set of halo CMEs (8.4%, or 26 of 309 halo CMEs observed by the LASCO in the 5 yr period) causes major geomagnetic storms. For the 27 major geomagnetic storms investigated, we find that 67% of them (18 events) are associated with full-halo CMEs and 30% (eight events) are with partial-halo CMEs. In comparison with all halo CMEs, 48% (149 events) are full-halo CMEs, and 52% (160 events) are partial-halo CMEs. Consequently, full-halo CMEs are more likely to cause major geomagnetic storms than partial-halo CMEs.

Second, we look into the CME speed measured at the Sun. We find that geoeffective CMEs can be from both fast and slow CMEs. Among the 26 events that have a measurable solar CME speed, 65% of them (17 events) have a speed greater than 500 km s^{-1}, while 35% (nine events) have a speed less than 500 km s^{-1}. In comparison with all 309 halo CMEs observed in the same period, 66% (203 events) have a speed greater than 500 km s^{-1}. Thus, it is clear that fast-halo CMEs are not more geoeffective than slow-halo CMEs. Nevertheless, we point out that on average the halo CME speed (720 km s^{-1} over 309 events) is larger than that of all CMEs (470 km s^{-1} on average over 3331 events). Earlier studies, which have used solar wind data as a proxy for solar CMEs, have suggested that major geomagnetic storms are caused by fast CMEs (Gosling et al. 1990; Tsurutani & Gonzalez 1998). However, our study presents a more diverse picture: a moderate percentage of slow-halo CMEs (36%) can cause major geomagnetic storms. Therefore, using fast-halo CMEs alone to predict major geomagnetic storms is not a sufficient criterion.

Third, we look into their association with other surface phenomena such as flares and erupting filaments. For the 27 major geomagnetic storms we investigated, only 30% (eight events) are associated with major flares (M- and X-class soft X-ray flares), and only 26% (seven events) are associated with erupting filaments. Erupting filaments (or disappearing filaments/erupting prominences) and eruptive flares have been widely used as CME proxies and related with magnetic clouds in interplanetary space (see, e.g., Joselyn & McIntosh 1981; Rust 1994). However, in terms of predicting major geomagnetic storms, they appear to be an unreliable indicator.

Based on the above discussions, there is no simple solar manifestation to predict that an ongoing solar halo CME will cause a major geomagnetic storm. CME speed, flare magnitude, or association with erupting filaments are not a good predictor of a CME's geoeffectiveness. The lack of solar manifestations of geoeffective CMEs poses a great challenge to space weather forecasting ability. Nevertheless, this result is understandable because these terms are not

related to the presence of prolonged strong southern magnetic field, which is a known key contributor to major geomagnetic storms.

5. CONCLUSIONS

Based on LASCO/EIT solar coronal observations, we have identified the solar sources of 27 major geomagnetic storms occurring between 1996 and 2000 inclusive; the other 11 major storms occurring in the same period are not investigated because of instrumental data gaps. Our approach to the identification consists of two steps. The first step is to use a fixed time window of 30–120 hr to select candidate front-side halo CMEs. The second step is to make use of solar wind data to provide further constraints. One of the constraints is to use the solar wind ICME speed to calculate an adaptive time window, which is based on the assumption that an initially fast solar CME would decrease its velocity in their transit from the Sun to the Earth. We finally find that 16 (59%) major geomagnetic storms are associated with unique FSH CMEs, six (22%) events are associated with multiple FSH CMEs, four events (15%) are associated with halo CMEs without any surface signature, and one event (4%) is caused by a CIR. The six multiple events show complex solar wind flows and complex geomagnetic activity, which are probably a result of multiple halo CMEs interacting in interplanetary space. The surface sources of these complex events are prolific active regions that produce multiple CMEs within a short period. On the other hand, the four geoeffective CMEs without any surface signature are all partial-halo CMEs gradually emerging from the east limb. We believe that they are longitudinally extended CMEs. These CMEs' counterpart in the solar wind are found to be slow and long-period magnetic clouds with no companying shock.

We find a longitudinal asymmetry in source region distribution of the CMEs responsible for major geomagnetic storms. The geoeffective CMEs are more likely from the western hemisphere than from the eastern hemisphere. Excluding the four limb events of unknown surface source, geoeffective CMEs cover a longitudinal range from E50° to W80°; most of them (17 of 22, or 77%) are within a narrow longitudinal range from E20° to W50°. In terms of latitude, geoeffective CMEs originate within a latitude strip of between S50° to N30°. A majority of events (20 of 22 FSH CMEs) are from a latitude strip of ±30°.

CMEs have an average transit time of 64 hr (maximum 118 hr and minimum 31 hr) from the Sun to arrival at the near-Earth interplanetary space. The transit time from the Sun to the Dst peak time is 78 hr on average (maximum 135 hr and minimum 34 hr). There is a correlation between CME plane-of-the sky-velocity and CME transit time from the Sun to the near-Earth space. It can be simply described as $T = 96 - (V/21)$, where transit time T is in hours and the CME velocity is in kilometers per second.

We find that while most geoeffective CMEs are full-halo CMEs (67%) or partial-halo CMEs (30%), there is no simple solar manifestation to predict that an ongoing solar halo CME is geoeffective or not. There is no preference in terms of CME speed, magnitude of associated X-ray flares, and association with erupting filaments.

This work was supported at NRL by a grant from NASA. V. Bothmer acknowledges the support by the German Research Ministerium through the German Space Agency under project 50 OC 0005 (Stereo/Corona). *SOHO* is a project of international cooperation between ESA and NASA. The LASCO instrument was constructed by a consortium of the Naval Research Laboratory, University of Birmingham (United Kingdom), the Max-Planck-Institut für Aeronomie (Germany), and the Laboratoire d'Astronomie Spatiale (France). Statistical CME information is based on the CME catalog generated and maintained by the Center for Solar Physics and Space Weather, the Catholic University of America, in cooperation with NRL and NASA. We acknowledge the use of solar wind data from the on-line CDA Web site of NASA/GSFC. The *Wind* magnetic field and plasma data are courtesy of R. P. Lepping and K. Ogilvie, respectively. The *ACE* magnetic field and plasma data are courtesy of N. Ness and D. J. McComas, respectively. We acknowledge the use of geomagnetic data from NGDC. Magnetic cloud identifications are a courtesy of R. P. Lepping. J. Zhang thanks S. M. White for helpful discussions and careful reading of the manuscript and J. Morrill for his assistance in visiting NRL.

REFERENCES

Andrews, M. D., & Howard, R. A. 2001, Space Sci. Rev., 95, 147
Bothmer, V., & Rust, D. M. 1997, in Coronal Mass Ejections, ed. N. Crooker, J. Joselyn, & J. Feynman (Geophys. Monogr. 99; Washington, DC: AGU), 139
Bothmer, V., & Schwenn, R. 1994, Space Sci. Rev., 70, 215
———. 1995, J. Geomagn. Geoelectr., 47, 1127
———. 1998, Ann. Geophys., 16, 1
Brueckner, G. E., et al. 1995, Sol. Phys., 162, 357
———. 1998, Geophys. Res. Lett., 25, 3019
Burlaga, L. F., Behannon, K. W., & Klein, L. W. 1987, J. Geophys. Res., 92, 5725
Burlaga, L. F., Sittler, E., Mariani, F., & Schwenn, R. 1981, J. Geophys. Res., 86, 6673
Cane, H. V., Richardson, I. G., & St. Cyr, O. C. 2000, Geophys. Res. Lett., 27, 3591
Delaboudinière, J.-P., et al. 1995, Sol. Phys., 162, 291
Dungey, J. R. 1961, Phys. Rev. Lett., 6, 47
Fairfield, D. H., & Cahill, L. J. 1966, J. Geophys. Res., 71, 155
Gonzalez, W. D., & Tsurutani, B. T. 1987, Planet. Space Sci., 35, 1101
Gopalswamy, N., Lara, A., Lepping, R. P., Kaiser, M. L., Berdichevsky, D., & St. Cyr, O. C. 2000, Geophys. Res. Lett., 27, 145
Gopalswamy, N., Yashiro, S., Kaiser, M. L., Howard, R. A., & Bougeret, J. L. 2001, ApJ, 548, L91
Gosling, J. T., Baker, D. N., Bame, S. J., Feldman, W. C., Zwickl, R. D., & Smith, E. J. 1987, J. Geophys. Res., 92, 8519
Gosling, J. T., Bame, S. J., McComas, D. J., & Phillips, J. L. 1990, Geophys. Res. Lett., 17, 901
Gosling, J. T., & Pizzo, V. J. 1999, Space Sci. Rev., 89, 21
Howard, R. A., Michels, D. J., Sheeley, N. R., & Koomen, M. J. 1982, ApJ, 263, L101
Joselyn, J. A., & McIntosh, P. S. 1981, J. Geophys. Res., 86, 4555
Klein, L. W., & Burlaga, L. F. 1982, J. Geophys. Res., 87, 613
Landi, R., Moreno, G., Storini, M., & Antalova, A. 1998, J. Geophys. Res., 103, 20,553
Lepping, R. P., et al. 1995, Space Sci. Rev., 71, 207
Lindsay, G. M., Russell, C. T., & Luhmann, J. G. 1995, J. Geophys. Res., 100, 16,999
McAllister, A. H., Dryer, M., McIntosh, P., Singer, H., & Weiss, L. 1996, J. Geophys. Res., 101, 13,497
McComas, D. J., Bame, S. J., Barker, P., Feldman, W. C., Phillips, J. L., Riley, P., & Griffee, J. W. 1998, Space Sci. Rev., 86, 563
Ogilvie, K. W., et al. 1995, Space Sci. Rev., 71, 55
Richardson, I. G., & Cane, H. V. 1995, J. Geophys. Res., 100, 23,397
Rust, D. M. 1994, Geophys. Res. Lett., 21, 241
Sheeley, N. R., Jr., Walters, H., Wang, Y.-M., & Howard, R. A. 1999, J. Geophys. Res., 104, 24,739

Sheeley, N. R., Jr., et al. 1975, Sol. Phys., 45, 377
Smith, C. W., L'Heureux, J., Ness, N. F., Acuna, M. H., Burlaga, L. F., & Scheifele, J. 1998, Space Sci. Rev., 86, 613
Smith, E. J., & Wolfe, J. H. 1976, J. Geophys. Res., 3, 137
Subramanian, P., & Dere, K. P. 2001, ApJ, 561, 372
Tsurutani, B. T. 2001, in Space Storms and Space Weather Hazards, ed. I. A. Daglis (Dordrecht: Kluwer), 103
Tsurutani, B. T., & Gonzalez, W. D. 1998, in Magnetic Storms, ed. B. T. Tsurutani, et al. (Geophys. Monogr. 98; Washington, DC: AGU), 77
Webb, D. F., Cliver, E. W., Crooker, N. U., St. Cyr, O. C., & Thompson, B. J. 2000, J. Geophys. Res., 105, 7491
Weiss, L. A., Gosling, J. T., McAllister, A. H., Hundhausen, A. J., Burkepile, J. L., Phillips, J. L., Strong, K. T., & Forsyth, R. J. 1996, A&A, 316, 384
Zhang, J., Dere, K. P., Howard, R. A., Kundu, M. R., & White, S. M. 2001, ApJ, 559, 452